Scilight

Nanoenergy Communications

https://www.sciltp.com/journals/nc

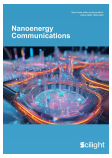

Review

Emerging DC-Generating TENG Mechanisms and Their IoT Applications

Sontyana Adonijah Graham [1,2], Andris Šutka [3] and Ju-Hyuck Lee [1,4,*]

[1] Department of Energy Science and Engineering, Daegu Gyeongbuk Institute of Science and Technology (DGIST), Daegu 42988, Republic of Korea
[2] KAIST InnoCORE PRISM-AI Center, Korea Advanced Institute of Science and Technology (KAIST), Daejeon 34141, Republic of Korea
[3] Institute of Physics and Materials Science, Faculty of Natural Sciences and Technology, Riga Technical University, P. Valdena 3/7, LV1048 Rīga, Latvia
[4] Energy Science and Engineering Research Center, Daegu Gyeongbuk Institute of Science and Technology (DGIST), Daegu 42988, Republic of Korea
* Correspondence: jhlee85@dgist.ac.kr

How To Cite: Graham, S.A.; Šutka, A.; Lee, J.-H. Emerging DC-Generating TENG Mechanisms and Their IoT Applications. *Nanoenergy Communications* **2026**, *1*(1), 3.

Received: 29 December 2025
Revised: 27 January 2026
Accepted: 5 February 2026
Published: 11 February 2026

Abstract: Direct-current triboelectric nanogenerator (DC-TENG) has emerged as a promising solution to power the rapidly expanding Internet of Things (IoT), by converting ambient mechanical energy directly into direct current (DC) output that is easier to store and manage than the alternating current (AC) signals of conventional TENGs. This review first introduces contact-electrification-based TENG fundamentals and maps how combinations with electrostatic induction, combined with various factors, lead to whether the output is AC, pulsed DC, or constant DC. Building on this foundation, emerging DC-generation mechanisms are organized into six classes: air-discharge dielectric breakdown, delay-switch and mechanical rectification, iontronic rectification, tribovoltaic junction, conductive dielectric, and ionic-dynamics/electrode-polarization effects. Their structural mechanism and their output relationships are clarified. Representative IoT applications domains of DC-TENGs are then highlighted, including human motion monitoring and wearable, smart agriculture and environmental monitoring, corrosion and cathodic protection, and electrochemical hydrogen generation, with emphasis on how DC characteristics simplify power management and enable self-powered sensing and communication. Finally, key challenges in materials, interfaces, device architecture, system integration, and standardization are summarized, and an outlook is provided on hybrid DC harvesters and co-designed electronics that could push DC-TENGs towards practical, large-scale IoT development.

Keywords: triboelectric nanogenerator; direct current; IoT applications

1. Introduction

The growth of IoT is driving a massive increase in low-power electronics applications for sensing, computing, and wireless communication [1–3]. Reliance on primary batteries for such applications leads to high maintenance costs, limited lifetime, and environmental concerns, motivating intensive research into ambient energy harvesting and self-powered systems. TENG, which converts mechanical stimuli into electricity via contact electrification and electrostatic induction, offers attractive features for IoT such as low cost, material and structural diversity, high voltage, and compatibility with flexible and wearable platforms [4–7].

1.1. IoT and the Need for Self-Powered Systems

Conventional TENGs are predominantly AC devices; periodic contact and separation of tribo-layers modulate interfacial charge distributions, resulting in high-voltage, low-current AC outputs that require rectification and power-management circuits before storage or use [4,8]. While this architecture has enabled numerous self-powered sensors and hybrid generators, the rectification stage introduces additional losses, complexity, and start-up overhead, especially problematic for ultra-low-power IoT applications operating irregularly [9]. DC-TENGs have therefore attracted growing attention as devices that can deliver predominantly unidirectional or constant-current output directly from mechanical motion, improving energy utilization and simplifying system-level integration [10].

1.2. DC-TENG Mechanisms and IoT Relevance

Recent works have shown that DC behaviour in triboelectric systems arises when contact electrification is coupled with additional interfacial or circuit phenomena that break the temporal and spatial symmetry of charge transfer [9,11]. Representative routes include air-discharge and electrostatic breakdown channels that convert otherwise dissipated corona into useful DC, mechanical time-delay switches and commutator-like electrode structures that release mechanical rectification, tribovoltaic effect at semiconductor p-n and Schottky junctions that generate DC via friction-excited carrier separation, phase-coupling and multi-unit designs that smooth output waveforms, and ionic or iontronic mechanisms that employ electrical double-layer (EDL) dynamics, ionic polarization, and rectification and liquid-solid or ion-polymer interfaces [12–14]. In parallel, progress in power-management circuits specifically tailored for DC-TENGs, such as dual-phase step-down converters and charge-space-accumulation schemes, is closing the gap between device-level physics and practical self-powered systems [15,16].

For IoT applications, DC-TENG offers several distinct advantages over AC-TENGs and many conventional mechanical harvesters [2]. First, direct DC output is inherently more compatible with energy storage elements (capacitors, supercapacitors, microbatteries) and with low-voltage electronics, reducing conversion stages and associated losses [12]. Second, some DC-TENG architectures, particularly tribovoltaic and certain air-discharge or ionic designs, can provide lower effective output impedance and more constant-current behaviour, which are beneficial for wireless transmitters, electrochemical systems, and sensor biases. Third, the high material properties from dielectrics and semiconductors to ionic gels and liquid interfaces enable application-specific optimization for wearable, harsh environments, or integrated chip-level systems [17]. In addition to powering IoT applications, the DC output of TENGs can be directly coupled with tribotronics and related semiconductor devices, enabling triboelectric or tribovoltaic potentials to modulate carrier transport in functional electronics [18,19].

1.3. Scope and Organization of This Review

This review summarized TENG fundamentals and discussed DC-TENG mechanisms from a device-physics perspective, but a focused view that connects emerging DC-generation pathways to IoT application requirements is still developing [6,10,12,13]. This review aims to fill the gap by (i) clarifying how constant electrification-based TENGs transition from AC to DC or constant-DC outputs when combining various factors; (ii) Organized emerging DC-TENG mechanism into six mechanisms-oriented classes, air-discharge dielectric breakdown, delay-switch and mechanical rectification, iontronic rectification, tribovoltaic junction, conductive dielectric, and ionic-dynamics/electrode-polarization; and (iii) mapping these mechanism classes onto representative IoT application domains such as human motion monitoring, smart agriculture and environmental monitoring, corrosion and cathodic protection, and hydrogen generation. Finally, the challenges and outlook section highlights key importance in materials, durability, standardization, and co-design with electronics, and outlines future directions towards scalable, robust DC-TENG-powered IoT infrastructure.

2. Contact-Electrification-Based TENG Mechanisms

In this review, the six “contact electrification + x” combinations in Figure 1 are defined by dominant additional physical pathways superimposed on contact electrification, namely (a) electrostatic induction; (b) electrostatic (air) breakdown; (c) quantum tunnelling; (d) p-n junction/Schottky junction fields; (e) phase control/mechanical delay switch; and (f) circuit-engineered rectification or charge pumping. Figure 1 schematically illustrates these contact-electrification-based TENG mechanisms and their electrical output at the core. Contact electrification at material interfaces generates static surface charge, which drives charge transport under changing geometry or boundary conditions, while the superimposed pathways (a–f) provide distinct routes for charge transfer away from the tribo-

charged interfaces. The resulting symmetry or asymmetry of charge transport in time and space determines whether the macroscopic output is predominantly AC, DC-biased, or nearly constant DC [13,14,20,21].

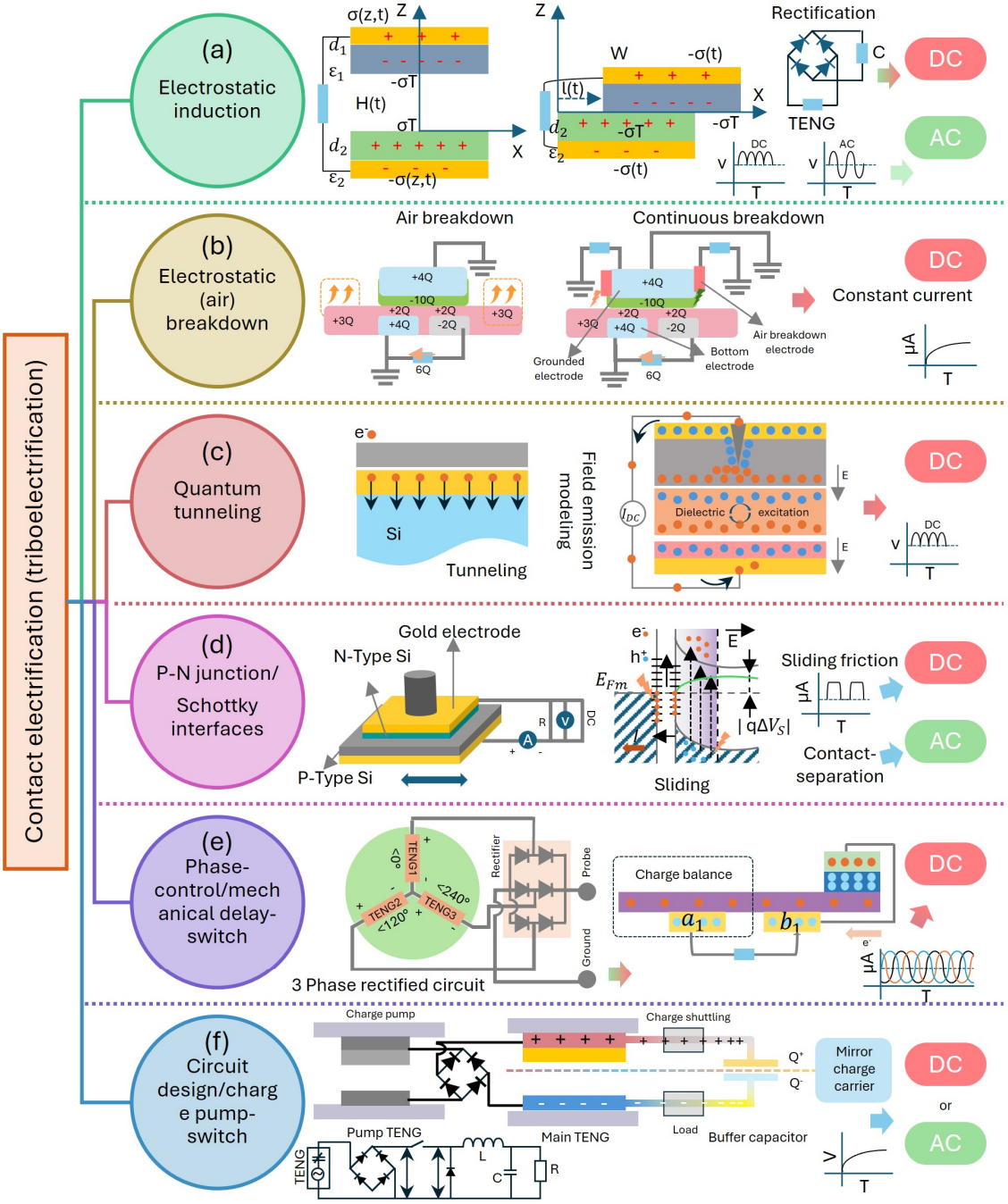

Figure 1. Contact-electrification-based TENG mechanisms showing a pathway towards producing AC or DC electrical output.

(1) Triboelectrification and Electrostatic Induction

In conventional TENG (Figure 1a), the coupling of contact electrification with electrostatic induction produces a time-varying potential difference as the electrodes move, leading to an AC output. Adding an external rectifier converts this AC into pulsating DC for energy storage or powering electronics [5,22]. From a mechanical standpoint, pure contact electrification plus electrostatic induction (Figure 1a) produces an AC output because the induced potential reverses sign during each approach/separation cycle. In each mechanical cycle, electrons are driven one way and then pulled back, so the current direction alternates and there is no net DC component if the motion is symmetric. When the AC source is followed by an electronic rectifier, the underlying induction remains symmetric, but the current constrains electron flow through the load to one direction, yielding pulsating DC [5,23,24].

(2) Triboelectrification and Electrostatic Breakdown

When contact electrification is coupled to electrostatic (air) breakdown, a high electric field exists between the tribo-charged dielectric and a nearby charge-collecting electrode that exceeds the breakdown strength of the medium and open corona/micro-discharge channels (Figure 1b). Electron flow through these channels always has the same direction, so individual breakdown events appear as unidirectional discharge pulses and, when discharge domains and motion are properly regulated and continuously sustained along the motion path, the combined effect can be engineered into a nearly constant-dielectric DC-TENG [21,25,26].

(3) Triboelectrification and Quantum Tunneling

At nanometer-scale gaps or ultrathin barriers, the contact-electrification-induced potential creates an extreme electric field across the gap, leading to high asymmetric quantum tunneling probabilities (Figure 1c) [13,15]. When the triboelectric potential exceeds a threshold, electrons favorably tunnel in one direction, so tribo-charges are released through a unidirectional tunneling current, and each mechanical cycle yields a net DC-based output, even though the mechanical motion itself remains periodic [27,28].

(4) Triboelectrification and p-n Junction/Schottky Interface

At the semiconductor p-n junction and Schottky interfaces, contact electrification coexists with a built-in electric field at the junction. Under vertical-separation, the motion mainly modulates the depletion-region width and interface potential, so the electrical signal is dominated by a tribo-electrostatic, AC-like output with an additional contribution from dynamic junction modulation rather than a purely DC tribovoltaic (Figure 1d) [29–32]. In contrast, under lateral sliding (tribovoltaic mode), friction excites electron-hole pairs at or near the junction, and the built-in field drives electrons and holes consistently towards the n- and p-sides (or metal and semiconductor), respectively; in a dynamic metal-semiconductor Schottky contact or sliding p-n junction, this continuous separation of friction-excited carriers yields a rectified DC output with relatively low effective impedance, often referred to as a sliding Schottky DC-TENG or tribovoltaic nanogenerator [33–35].

(5) Triboelectrification and Phase Control/Mechanical Delay Switch

For phase-control and mechanical delay-switch DC-TENGs (Figure 1e), multiple triboelectric units or electrode segments are engineered so that their AC outputs are intentionally phase-shifted in time, or their electrical connection to the external circuit is delayed to specific moments within the mechanical cycle. In multiphase designs, several TENG units with different contact positions or activation sequences generate AC current with controlled phase differences. When these phase-shifted outputs are superimposed and appropriately rectified, the positive portions partially fill each other's gaps, leading to a more continuous and less strongly pulsed DC output than that of a single-phase TENG [36]. In mechanical delay-switch structures, an internal mechanical commutator or time-delay contact selectively connects the tribo-charged elements to the load only during the portion of the cycle that drives electrons in one preferred direction, thereby releasing an intrinsic mechanical rectification that produces a single-channel DC output while minimizing losses in conventional diode rectifiers [37].

(6) Triboelectrification and Circuit Design/Charge Pump-Switch

When contact electrification and electrostatic induction or controlled breakdown paths are combined with tailored circuit architectures (e.g., charge-pumping, rectifier network, synchronous-switch schemes), the external network imposes directionality on the current through diodes or time-controlled switches (Figure 1f). As a result, the same underlying mechanical waveform can be engineered to yield predominantly AC, pulsed AC, or nearly constant DC outputs, depending on device geometry, load configuration, and the specific power-management topology employed [12,13,15].

In summary, Figure 1 shows the schematic illustration of contact-electrification-based TENG mechanisms and their electrical output. At the core, contact electrification at material interfaces generates static surface charges, which drive charge transport under changing geometry or boundary conditions. Building on this common origin, Figure 1 highlights how different DC-generation routes progressively break the symmetry of the basic contact electrification process, shaping the same interfacial charge into AC, DC-biased, or constant-DC outputs and providing the basis for the classification under the following sections.

3. Emerging DC-Generation Mechanisms in Triboelectric Nanogenerator and Their Overview

(1) Air Breakdown

Figure 2 shows the emerging DC-generating mechanisms in TENGs and their overview. Early studies in the TENG field largely treated air breakdown as a limiting factor that suppressed charge density and reduced output performance, and research initially focused on understanding and optimizing TENG performance under this

constraint. In 2018, Luo et al. first demonstrated the concept of using air breakdown as part of the working mechanism to create a direct-current (DC) output by intentionally forming an ionized air channel during operation, thereby shifting the focus from limiting the use of air discharge phenomena [38]. Building on this, Yoon et al. reported a micro discharge-based DC-TENG that harnesses controlled atmospheric air breakdown to generate continuous DC output with significantly enhanced current density, establishing air discharge as an active mechanism for energy harvesting rather than just a loss process [39]. Following these foundational works, the field has diversified and matured. Researchers now explore both structural suppression/inhibition of undesirable air breakdown to boost charge density and performance in conventional TENG architecture, as well as novel air-discharge-enabled devices for specific applications. Recent work, such as the electrostatic breakdown DC-TENG reported by Zhang et al. demonstrates optimized high-voltage air discharge control, achieving open-circuit voltage up to ~18 kV and enabling practical applications like self-powered air purification systems by generating a large number of negative air ions [40]. Figure 2a illustrates a double-output-mode TENG in which triboelectrification/contact electrification is combined with corona/air-discharge effect to release a DC output [41]. In a conventional high-charge AC-TENG, once the local electric field at the dielectric surface exceeds the breakdown strength of air (~3 kV mm^{-1}), ionization leads to uncontrolled air breakdown that dissipates accumulated charges and limits surface outputs. In the air-discharge DC-TENG architectures, an additional "air-breakdown" collecting electrode is deliberately introduced opposite to the charged tribo-layer across a designed air gap, so that the electrostatic breakdown pathways are harnessed to extract rather than lose these charges, producing a unidirectional DC current. The air gap between the dielectric tribolayer and the metal breakdown electrode is therefore a critical design parameter; it must be small enough to generate a sufficiently high field for stable ionization and air-channel formation, yet large and uniform enough to avoid hard arcing and mechanical contact [21,38,42]. The 3D structure diagram and photographic images show that such DC-TENGs can be implemented in sliding and rotary double-output-mode TENG configurations, with patterned electrodes that define separate AC-output and DC-collection regions to increase effective surface charge utilization. By rationally patterning the electrodes and optimizing the charge-space accumulation area, the air-discharge path captures dissipated charge that would otherwise be lost, thereby significantly increasing the effective DC charge density and enabling nearly constant-current behaviour under steady motion. However, these devices also exhibit characteristic limitations: (i) Severe wear and durability issues due to the need for high surface charge density and strong friction; (ii) essentially one-polarity DC output for simple configuration; (iii) strong dependence on ambient conditions such as humidity, which alter the breakdown field and discharge dynamics; (iv) strict requirements on maintaining a well-controlled gap and friction interface geometry; and (v) relatively high internal resistance inherited from the dielectric materials and ionized air channel [12,21,22,38].

(2) Delay Switch and Mechanical Rectification

Early work on DC-TENGs using mechanical rectification and delay switching mainly focused on proving that purely mechanical elements could replace electronic diode bridges to impose unidirectional charge transfer on an intrinsically AC triboelectric source. In 2021, Qiao et al. first proposed a bidirectional direct-current TENG with a mechanical rectifier (BD-TENG), where a commutator and rolling brush structure converted the alternating output of the triboelectric unit into DC without any electronic rectification, demonstrating mechanical rectification as a viable route to DC output [43]. Subsequently, Wu et al. introduced a mechanical delay-switch DC-TENG inspired by transistor operation [44]. followed by Du et al.'s mechanical time-delay switch with charge space-accumulation design, which significantly improved average power density and durability by accumulating charge over a blank tribo area and releasing it through a unidirectional mechanical switch. Figure 2b illustrates a mechanically rectified DC-TENG in which the time-controlled electrode switching and structure design convert the inherently alternating triboelectric potential into a net unidirectional charge flow, without using conventional electrode diodes [45]. In the linear MDC-TENG unit, a slider carrying (or not carrying) a dielectric layer sequentially passes over patterned stator electrodes and a blank tribo-area, forming a mechanical time-delay switch. During one part of the movement, only one electrode is effectively coupled to the tribo-charged surface, while in the delayed region, the connection is transferred to the other electrode. This continuous exchange of effective electrode positions relative to the charged area causes electrons to always flow in the same direction through the external circuit, thereby achieving mechanical rectification of the triboelectric output [13,15].

The 3D structural schematic without and with dielectric (e.g., FEP) on the slider, together with the simplified working-principal diagram under charge saturation, clarifies how introducing the dielectric on the slider enhances charge accumulation and stabilizes the delayed switching behavior. Measured current and dynamic charge curves at two electrode pairs (e.g., at 2 Hz) show that, although each individual electrode experiences alternating local potentials, the combined effect of the time-delay region and electrode sequence yields a unidirectional current. By

adding extra sliding distance (blank region), the effective delay time between switching events can be adjusted, which strongly affects the DC level and wave of the output, as summarized by the dependence on extra sliding range [15,45].

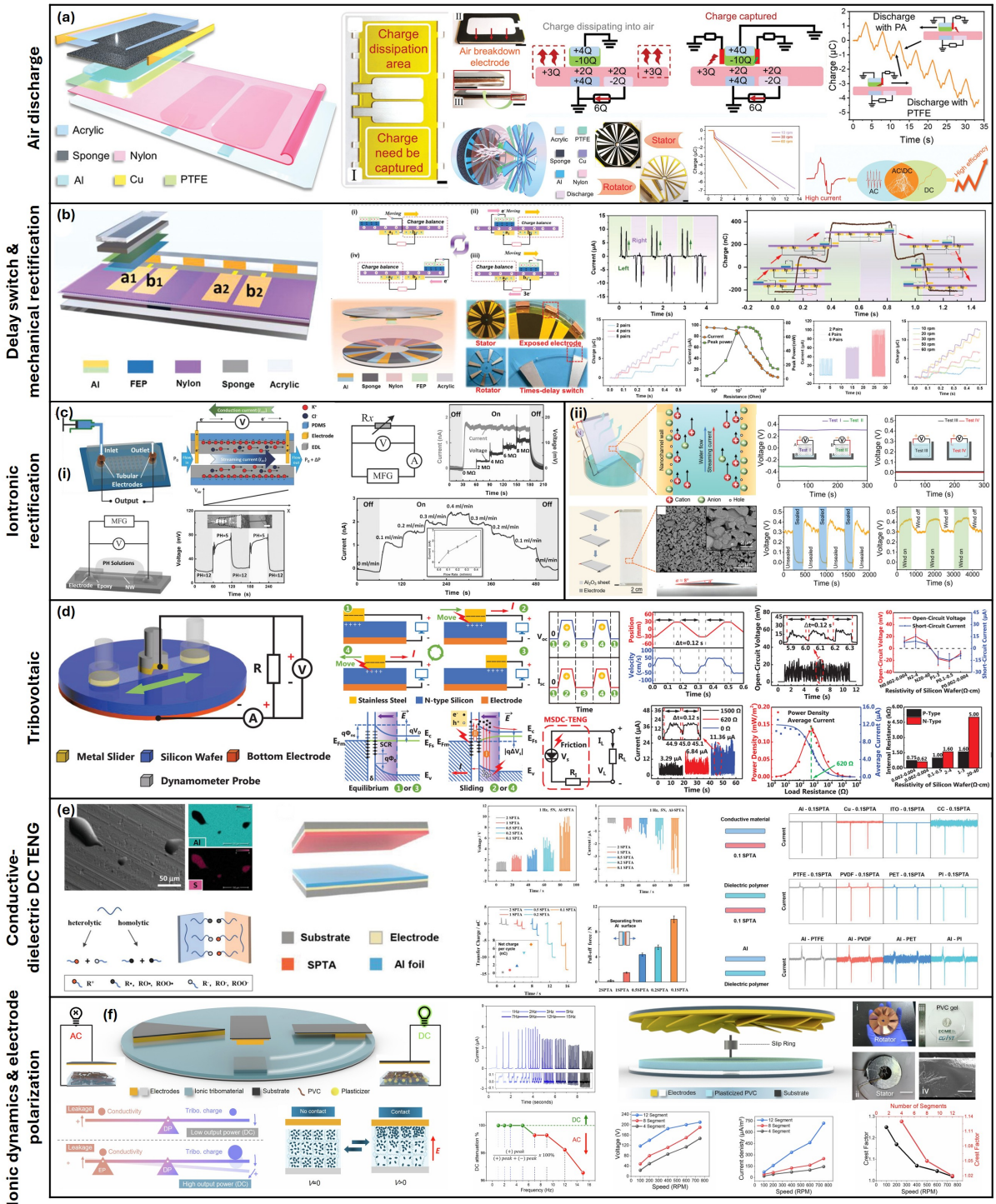

Figure 2. Emerging DC-generation mechanisms in triboelectric nanogenerator and their overview. (**a**) Air breakdown mechanism, adopted with permission from [41], © 2022 Wiley-VCH GmbH. (**b**) Delay switch and mechanical rectification, adopted with permission from [45], © 2022 Wiley-VCH GmbH. (**c** (**i** and **ii**)) Iontronic rectification, adopted with permission from [46,47], © 2015 WILEY-VCH Verlag GmbH & Co. KGaA, Weinheim, and © 2022 Wiley-VCH GmbH. (**d**) Tribovoltaic, adopted with permission from [48], © 2020 WILEY-VCH Verlag GmbH & Co. KGaA, Weinheim. (**e**) Conductive-dielectric DC-TENG, adopted with permission from [49] © 2024 Wiley-VCH GmbH. (**f**) Ionic dynamics and electrode polarization, adopted with permission from [14] Copyright © 2025 Springer Nature.

The rotational MDC-TENG is further released by arranging multiple electrode-switch segments around a rotor, where the rotation inherently implements a periodic, phase-shifting mechanism switching between electrode pairs. 3D schematics and device photographs (stator, rotor, enlarged electrode switches) show that this design generalizes the linear concept into a compact rotary form. The measured charge, current, and open-circuit voltage at different rotation speeds, together with matching impedance and power curves, demonstrate that the rotational MDC-TENG can deliver competitive average power density related to other DC-TENG architectures. The underlying mechanism can be viewed as a triboelectric analogue of a mechanical transistor, where the controllable parameters are the same time (delay) and spatial structure of electrode engagement. However, the approach also brings characteristic limitations, such as wear of sliding/switching electrodes (leading to output noise), complex mechanical design requirements for reliable switching, high internal resistance from dielectric layers, sensitivity to frequency/oscillation conditions, and durability challenges due to multiple moving and electrically contacting parts [13,15].

(3) Iontronic Rectification

Figure 2c summarizes the DC generation mechanism in which ionic motion and electrical double layer (EDL) rectification at liquid-solid interfaces convert flow- or evaporation-driven potentials into a net DC output, often termed triboiontronic or iontronic TENG systems [50–52]. Early work, such as that by Zhang et al. in 2015, established that liquid-solid streaming potential in microfluidic channels can provide continuous DC power for self-powered nanosystems.[46] Moreover, recent studies, exemplified by Chi et al. generalize this concept to liquid-solid TENG architectures driven by natural water evaporation, achieving robust, steady DC outputs for low-power electronics and demonstrating the broader potential of liquid-based DC triboelectric systems [47]. (Figure 2(ci)) In a streaming-potential-based microfluidic generator (MFG), pressure-driven liquid flow through charged nanochannels drags counterions in the EDL, creating a streaming current and potential along the channel. By connecting the two ends through an external circuit, a unidirectional ionic current and corresponding DC electrical output are obtained, with magnitude and polarity governed by flow direction, channel surface charge, and ionic strength. Voltage-current characteristics and short-circuit current measurements under forward and reverse flows demonstrate clear rectification behaviour, the current sign reverses with flow direction, and the current scales approximately linearly with flow rate over a practical range, enabling self-powered operation of nanoscale sensors such as ZnO nanowire pH detectors without external bias [46].

Figure 2(cii), shows the water-evaporation-driven liquid-solid TENGs extend this concept by using capillary flow and continuous evaporation to maintain a steady ionic flux through porous, charged membranes (e.g., Al_2O_3 sheets), where the formation and disruption of EDLs along nanochannels induce a persistent streaming potential. In such devices, natural water evaporation maintains an upward ionic flow that generates a DC voltage between electrodes on opposite sides of the membrane. Systematic tests under different orientations, immersion states, sealing conditions, and air flow confirm that the output originates from evaporation-induced liquid motion rather than simple electrochemical or thermoelectric effects [47]. Consequently, these ionotropic systems can be viewed as TENG-like interfaces in which the primary mobile charges are ions, and rectification arises from asymmetric EDL dynamics and channel geometry, but they also suffer from characteristic limitations, including relatively low and sometimes unstable DC output, complex multiphysics mechanisms, and materials requirements, sensitivity to environmental conditions (humidity, temperature, ionic composition), and challenges in achieving long-term uniform performance due to liquid handling and interface degradation [50,51,53].

(4) Tribovoltaic

Figure 2d illustrates a metal-semiconductor-based DC TENG (MSDC-TENG), in which sliding friction at a metal-semiconductor (MS) interface excites electron-hole pairs that are separated by the built-in electric field of the junction, giving a low-impedance DC output via the tribovoltaic effect. Early work on tribovoltaic DC-TENGs focused on proving that sliding at semiconductor junctions can directly generate true DC rather than AC-type triboelectric signals. In 2020, Zhang et al. first established the tribovoltaic effect at metal-semiconductor interfaces, showing that lateral sliding across a Schottky junction produces a steady DC output driven by built-in fields and friction-induced carrier excitation, which clearly differentiates tribovoltaic DC generation from conventional triboelectrification [48]. Subsequently, studies systematically generalized this concept to various semiconductor interfaces and device architectures [17,35]. Recent theoretical works and device advances towards ultrahigh-current-density organic and inorganic heterojunctions have shifted the field towards quantitative modeling, interface engineering, and high-performance, application-oriented tribovoltaic DC-TENG [33,54]. In the Figure 2d, the 3D schematic of the measurement setup and external circuit shows a metal slider moving periodically across a doped silicon wafer, the relative position and velocity versus time define the sliding period during which a continuous open-circuit voltage is observed, rather than a discrete AC pulse typical of conventional TENGs. The output

characteristics confirm DC behaviour, the open-circuit voltage maintains a nearly unipolar signal over each sliding interval Δt, and the measured current under different load resistance (e.g., 155, 620, and 0 Ω) provides an impedance-matching curve from which power density and average current as a function of load can be extracted, demonstrating much lower impedance than regular dielectric-based DC-TENGs. The band diagram analysis explains the mechanism. In equilibrium, the MS junction forms a Schottky barrier (work function of metal Wm > Ws) under sliding, frictional interaction at the interface supplies energy to generate an electron-hole pair, and the junctions built-in field drives electrons and holes in opposite directions across the barrier, producing a net DC current similar to the photovoltaic effect but driven by mechanical friction rather than light [55].

The working-cycle schematics and equivalent circuit model show the contact electrification at the interface coexist with tribovoltaic carrier generation, but the domain DC pathway arises from the friction-induced excitation and built-in-field separation of carriers, which makes tribovoltaic DC-TENGs structurally compatible with semiconductor electronics and promising for low-impedance, IC-level self-powered systems. At the same time, this mechanism entails characteristic constraints, the need for semiconductor materials (with their limited flexibility and transparency), and typically moderate output voltage compared with air-breakdown DC-TENGs, sliding-induced wear and durability issues, and an as-yet incomplete understanding of interfacial physics that currently restricts optimization strategies and the exploration of compressive/contact-separation tribovoltaic architecture [17,31,35].

(5) Conductive Dielectric

Figure 2e shows a DC-TENG that operates in the contact-separation mode but uses a conductive-adhesive polymer interface (e.g., SPTA-stabilized poly(thioctic acid) on Al) to release asymmetric charge generation and leakage, thereby converting the usual AC-like TENG output into a DC-dominated signal. Early work on conductive-dielectric/interfaces in TENGs mainly focused on showing that introducing a finite conductivity or conductive/adhesive path could reshape charge transfer and enable rectifier-free DC output even in contact-separation mode. In 2024, Shi et al. demonstrated a DC-TENG based on a conductive-adhesive interface, where the engineered conductive/ionic adhesive layer suppresses one half-cycle and allows charge transfer predominantly in a single direction, releasing intrinsic DC output without electronic rectifiers [49]. Subsequent studies, using porous volume-conductive or semi-conductive dielectric and internal transport pathways to achieve constant DC output with ultrahigh power density, indicate a clear trend towards architecting conductive and conductive adhesive dielectrics as active functional elements in high-performance DC-TENGs [56]. In Figure 2e, the device structure consists of an Al foil electrode modified with different self-polymerised thioctic acid (SPTA) adhesives and a counter electrode. Output voltage and current measurements at 1Hz and 5N show that certain SPTA formulations produce distinctly different waveforms and average current levels compared with purely dielectric or purely conductive interfaces [49].

By analyzing applied forces of various SPTA adhesives on Al and correlating them with transferred charge, the study confirms significant material transfer during contact electrification, and points to adhesion strength as a key parameter controlling mechanoion generation via covalent bond cleavage at the interface. The transfer charge, together with the SEM and EDS analyses of the Al surface rubbed with 0.1 SPTA, supports a mechanism in which covalent bonds in the SPTA layer cleave (heterolytic or homolytic pathways), generating ionized particles that contribute to charge accumulation and, importantly, to direct-dependent charge leakage with the conductive and dielectric components are combined.

Comparative output characteristics of TENGs with conductive-SPTA, dielectric-polymer-SPTA, and hybrid conductive-dielectric polymer interfaces reveal that the conductive-dielectric configuration provides the most favorable balance of high adhesion, low leakage through unwanted channels, and asymmetric surface geometry. Consequently, this conductive-dielectric DC-TENG can be viewed as a mechanoion-generation-assisted triboelectric device, where covalent-bond cleavage and charge-leakage pathways at an engineering adhesive interface replace more classical routes like air breakdown or semiconductor junction fields. However, the approach is still constrained by the need for specific adhesive chemistries, relatively low and condition-sensitive output stability, complex interfacial mechanisms, and durability concerns associated with repeated material transfer and adhesion-controlled contact [5,13,57].

(6) Ionic Dynamics and Electrode Polarization

Figure 2f dispites an ion-based DC-TENG (iDC-TENG) where ionic dynamics and electrode polarization in a PVC gel layer are used to convert the usual AC-like triboelectric signal into a DC-dominated output in contact-separation, sliding, and rotary modes. Early studies on ionic effects in triboelectric devices mainly showed that introducing mobile ions and enhancing electrode polarization could dramatically modify charge transport and output, but the generators still behaved essentially as AC sources. Researchers demonstrated that controlling the

ionization of functional groups and electric-double-layer formation in polymer dielectrics strongly affects charge accumulation, screening, and stability, thereby establishing ionic polarization and electrode polarization as active design parameters in TENG engineering [58,59]. Most recently, in 2025, Gbadam et al. reported the first DC-TENG in which ionic dynamics and electrode polarization are identified as the dominant DC-generational pathways, showing that appropriately formulating ionic tribomaterials can convert a conventional AC-TENG into a rectifier-free iDC-TENG with stable DC output across contact-separation, sliding, and rotary modes. This marks a clear trend towards harnessing ionic motion and electrode polarization to release a robust DC-TENG system [14]. In this architecture, a polyvinyl chloride (PVC) gel containing an ionic plasticizer (e.g., DOA) is used as the tribo-layer, under constant electrification with a counter electrode, the induced electric field polarizes mobile ions inside the gel, driving them towards or away from the interfaces and establishes a built-in ionic polarization that persists over a relaxation time much longer than the mechanical contact event. The schematic lever diagram summarizes the relationship between film conductivity and power output, as ionic conductivity increases from purely dielectric towards optimally ion-conducting PVC gel, ionic displacement under the triboelectric field enables a net DC bias, whereas too high conductivity leads to rapid charge dissipation and loss of output.

The working mechanism schematic for contact-separation, sliding, and rotary iDC-TENGs shows that, during contact, triboelectric charges on the solid interface create an electric field that polarizes ionic particles within the gel, during separation, the slow relaxation of this ionic polarization and associated electrode polarization causes asymmetrical charge exchange with the electrodes, leading to unidirectional or DC-biased current pulses instead of symmetric AC peaks. This transition from AC to DC behaviour is experimentally demonstrated by short-circuit current output of PVC films with different DOA contents as the plasticizer ratio (and ionic mobility) increases, the waveform gradually evolves from symmetric bipolar peaks to predominantly single-polarity peaks. Frequency-dependent measurements further reveal that at low frequencies, the polarization and relation balance favor DC-dominated output, while at higher frequencies, the limited time for ionic rearrangement leads to partial recovery of AC behaviour, which is quantified by the changing ratio of contact to separation peak amplitudes and a defined DC weakening measured.

A flap-based rotary iDC-TENG (iDC-RTENG) is then implemented by incorporating large-area PVC gel films into a segmented rotor-stator structure. 3D schematics and photographs of the rotor, stator, and gel cross-section illustrate the scalable design. Electrical measurements of the iDC-RTENG show that, with 12 segments at 750 rpm, the device delivers a stable DC open-circuit voltage over 10^5 cycles, and the short-circuit current and voltage scale with rotation speed from 100 to 750 rpm while maintaining a relatively low crest factor for appropriately chosen segment numbers, indicating smooth DC output. Overall, this ionic dynamic and electrode polarization route can be regulated as an emerging interfacial iontronic DC-TENG mechanism, where the DC character stems from slow ionic polarization/relaxation rather than air-breaking down or semiconductor junction fields, but it also inherits challenges such as sensitivity to frequency and temperature, and the need to finely tune ionic conductivity and gel composition for long-term stable operation [14].

(7) Other Hybrid Mechanism: Liquid/Ionic Conduction-Current DC Mechanism

Recent work has shown that, in liquid-solid systems, DC output can arise from conduction-current-dominant pathways that are superimposed on conventional contact electrification. In a bio-inspired “total current nanogenerator”, Dong et al. designed a droplet-based liquid-solid TENG in which both displacement current and liquid-phase conduction current are harvested to deliver high-voltage DC output without external rectification, providing a clear example of conduction-assisted DC generation beyond pure electrostatic induction [60]. Liu et al. further developed liquid-solid triboelectric probes that resolve interfacial charge transfer and current signals in real time, demonstrating how ionic composition, concentration, and flow state govern the balance between displacement and conduction currents at the liquid-solid interface and can give rise to direction-preferential, rectified-like outputs under appropriate operating conditions [61]. Besides, a thunderbolt-inspired droplet-based DC generator shows that repeated droplet impact, interfacial charge separation, and guided charge extraction in a conductive liquid path can produce high-voltage DC at the solid-liquid interface, confirming that conduction-current mechanisms provide a practical route to DC generation in a droplet-based TENG [60]. Within the framework of Figure 2, these liquid-solid systems are categorized under the iontronic rectification, conductive dielectric DC-TENG, and ionic dynamics and electrode polarization routes, where ionic motion, interfacial polarization, and controlled conduction pathways play a central role in establishing a net DC electrical output.

4. IoT Applications of DC-TENG

(1) Human Motion Monitoring

Figure 3 shows the IoT applications of DC-TENG. Figure 3a presents the multifunctional self-charging system in which a fabric-based P/N-type DC-TENG serves simultaneously as a human-motion energy harvesting and motion sensor, enabling continuous charging of small electronics and real-time motion monitoring for wearable IoT applications. The preparation process and structural design schematics show a compatible electrode configuration, where p-type and n-type fabric layers form a P/N -type DC-TENG that generates friction current during body movements. A charge-transfer diagram for two contact states clarifies how asymmetric charge transport at the P/N interface leads to a net DC output rather than a purely AC signal.

Figure 3. IoT applications of DC-TENG. (**a**) Human motion monitoring, adopted with permission from [62] Copyright © 2025, American Chemical Society. (**b** (**i** and **ii**)) Smart agriculture and environmental monitoring, adopted with permission from [45,63], © 2022 Wiley-VCH GmbH, and © 2022 Springer Nature. (**c**) Corrosion protection and cathodic protection, adopted with permission from [64], © 2025 Wiley-VCH GmbH. (**d**) Hydrogen generation, adopted with permission from [65], © 2025 Wiley-VCH GmbH.

A conceptual diagram of the motion-monitoring process illustrates that different human actions (e.g., walking, running, or specific limb motion) modulate the contact frequency, contact area, and pressure on the fabric TENG, which in turn changes the amplitude and time-based pattern of the DC output, allowing the electrical signal to encode motion information. The self-charging equivalent of a circuit diagram shows the DC-TENG connected to rectification/management elements and a strong component (e.g., commercial capacitors), forming a self-sustained power unit that can charge devices such as a small timer without external power. Experimental plots of output voltage and current under different motion states, together with capacitor-charging curves and demonstration of timer operation, confirm that the DC-TENG can both power low-power wearable electronics and sense motions, highlighting its suitability as a human-centric IoT application [62,66,67].

(2) Smart Agriculture and Environmental Monitoring

Figure 3b illustrates how high-performance DC-TENGs, such as the mechanical-delay-switch MDC-TENG and rotary primary-cell-inspired (R-PC-TENG), can act as a distributed power hub for agriculture and environmental IoT applications, harvesting ambient mechanical energy (water flow, wind, rotation) to drive sensing and communication devices in the field. In the MDC-TENG system, coupled to an energy-management unit (EMU) that rectifies, stores, and conditions the DC output, circuit diagrams, photographs, and capacitor-charging curves show that this configuration can light thousands of LEDs, charge capacitors at 60 rpm, and continuously power Bluetooth hydrographs and multiple hydro-thermometers monitoring temperature and humidity, demonstrating its suitability for self-powered microclimate and environmental monitoring [45]. Similarly, the R-PC-TENG, inspired by the architecture of a primary cell, is integrated into a self-powered system with power-management circuitry that harvests wind energy to charge capacitors while simultaneously driving infrared transmitting modules and several hydro-thermometers, enabling wireless environmental sensing and data transmission without external power. System-level schematic and application photos highlight that this DC-TENG platform can be deployed on water pipes, wind-exposed structures, or agricultural installations, where its high durability and stable DC output support networks of distributed sensors (e.g., humidity, temperature, or other environmental parameters), aligning directly with smart agriculture and environmental IoT applications [63].

(3) Corrosion and Cathodic Protection

Figure 3c, corrosion and cathodic protection powered by DC-TENG-based hybrid harvester. Figure 3c shows a dual-effect direct-current ocean-energy harvesting system in which a triple-dielectric DC-TENG (TDC-TENG) is combined with a solid-state thermoelectric generator (SS-MTEG) to provide a more stable DC output suitable for cathodic protection and corrosion mitigation in marine environments. The prototype structure and application-scenario diagram depict TDC-TENG units that harvest low-frequency mechanical excitation (e.g., wave or structural motion) and SS-MTEG units that exploit temperature gradients, whose outputs are merged via an energy-management unit to form a composite DC source. Open-circuit voltage, short-circuit current, and transferred charge measured at different rotation or wave-simulated speeds demonstrate that the hybrid harvested maintains an applicable DC level across various conditions.

The double-effect DC composite energy harvesting prototype and its experimental system photographs illustrate integration of the TDC-TENG/SS-MTEG stake with power-conditioning circuitry and a corrosion-protection load, enabling improved-current cathodic protection of metal structures by supplying a continuous negative potential to the protected surface. By leveraging the high-voltage, mechanically driven DC from the triple-dielectric TENG together with the more continuous thermoelectric contribution, this architecture improves energy availability and stability for long-term cathodic-protection applications on ocean-exposed components such as pipelines, platforms, or mooring elements, reducing dependence on external power or sacrificing anodes [64].

(4) Hydrogen Generation

Figure 3d illustrates a DC-TENG power system in which a surface non-equilibrium state, induced by unipolar charge collection, is used to construct a constant-current DC-TENG (DSC-TENG) that can directly drive hydrogen evolution and low-power wireless electronics. The output-power curves under various external loads and the associated power management circuit show that the DSC-TENG delivers a relatively stable current over a broad load range, with an electrical output that can be interpreted as an asymmetric AC signal composed of a dominant DC component plus a small symmetric AC part, making it well suited for electrochemical processes requiring stable current.

A schematic of the hydrogen-evolution setup and application scenarios demonstrates that the DSC-TENG power system (with its charging-discharging behaviour characterized by capacitor curves) can act as the sole power source for water electrolysis, continuously generating hydrogen at the electrodes without an external supply. In parallel, wireless-transmission applications diagram and experimental results show that the same DSC-TENG

array can power a wireless transmitter and allow the receiving end to successfully decode a message, underscoring the dual functionality of this constant-current DC-TENG platform for both hydrogen generation and self-powered wireless IoT communication in integrated energy-harvesting systems [65].

5. Challenges and Future Prospects

5.1. Materials, Interfaces, and Durability

Despite rapid progress, many DC-TENG mechanisms rely on aggressive interfacial conditions, strong friction, high surface charge density, repeated air breakdown, or sliding semiconductor and ionic interfaces, which raise durability concerns. Wear of triboelectric layers and electrodes, degradation of semiconductor junctions in tribovoltaic devices, and mechanical lower durability or dehydration in ionic gels can cause performance drift and eventual failure, especially under real-world vibrations, temperature, and humidity cycles. Developing wear-resistant tribomaterials, robust encapsulation strategies, and self-healing or replenishable interfaces will be essential for long-term IoT deployments [12,14,17,21,68].

Fundamental understanding of interfacial charge transfer, especially in complex systems such as tribovoltaic contacts, mechanoion-generating adhesive interfaces, and iontronic or ion-polarization-based DC-TENG, remains incomplete. More quantitative models that couple mechanical, charge transport, chemical reactions, and ion dynamics are needed to guide rational optimization, including trade-offs between conductive and charge retention, or between high field strength and breakdown control. Advanced in-suit characterization of charge distributions, discharge domains, and interfacial chemistry will play a critical role here [14,15,25,35].

5.2. Device Physics Perspective

From a device-physics perspective, advancing DC-TENGs will require closing the gap between microscopic interfacial processes and macroscopic output characteristics. First, quantitative relationships need to be established between interfacial charge-transfer mechanisms (including electron tunneling, carrier injection across built-in junction fields, and ion migration/polarization) and measurable DC figures or metrics such as current density, crest factor, and stability under realistic mechanical pressures [21]. Second, unified multi-physics models that self-consistently couple triboelectrification, built-in semiconductor or Schottky fields, electrostatic breakdown, ionic dynamics, and external circuit/load effects are needed to describe different DC-TENG architectures within a common framework and to enable predictive device optimization rather than observed tuning [69]. Third, there is a pressing need to engineer intrinsically unidirectional conduction paths through junction engineering, iontronic/electrode-polarization effects, conductive or adhesive interfaces, and hybrid semiconductor-ionic structures so that the same mechanical waveform can be deterministically shaped into stable, high-power DC output across a broad range of amplitudes and frequencies [14,45].

5.3. Stability and Environmental Robustness

For practical deployment, DC-TENG must maintain stable output under variations in temperature, humidity, and environmental contamination, yet systematic studies on long-term stability are still limited compared with those on AC-type TENGs. Humidity can screen surface charges, enhance leakage along surfaces, and strongly disturb air-discharge or corona processes, leading to a large drop in effective DC and accelerated performance degradation, while temperature cycling and dust can induce material fatigue, wear, and changes in triboelectric polarity or junction behavior. Recent work on waterproof/humidity-resistant and high-temperature TENGs suggests several mitigation strategies that are directly transferable to DC-TENGs, including robust encapsulation and sealing of air-discharge gaps, hydrophobic or self-cleaning coatings to suppress moisture adsorption and contamination, selection of thermally stable tribo-layers and conductive dielectrics, and lubrication or surface-engineering approaches that simultaneously reduce wear and stabilize sliding DC outputs. Establishing DC-TENG-specific durability protocols e.g., standardized cycling tests under controlled humidity/temperature after long-term operation, will be an improvement step towards qualifying DC-TENGs for real outdoor, wearable, and industrial environments [12,70–75].

5.4. Output Control and Standardization

Compared with well-established energy harvesters, DC-TENGs lack standardization test protocols and figures of merit that reflect realistic IoT loading conditions and operational cycles. Reported performance metrics often vary in terms of mechanical excitation, load definition, and data analysis, making cross-comparison between mechanisms (air-discharge, mechanical rectification, tribovoltaic, iontronic, etc.) difficult. Establishing

community-accepted standards for mechanical input, electrical load lines, power density normalization, and long-term stability testing will be crucial to assess which DC-TENG architectures are truly competitive for given IoT scenarios [6,12,76,77].

Precise control over output waveform (DC level) and internal impedance is also a challenge, yet these parameters directly affect compatibility with signaling modules, sensor front ends, and electrochemical loads such as corrosion protection or hydrogen evolution. Mechanism-specific strategies, e.g., phase-coupled multi-unit arrays, optimized mechanical delay-switch timing, air-discharge domain engineering, or ionic-conductivity tuning, need to be further explored to tailor DC-TENG outputs to particular IoT protocols and electronics [12,15].

5.5. Standardization of DC-TENG Test Protocols

Although this review briefly notes the lack of standardized testing for DC-TENGs, a more rigorous and comparable evaluation framework is still largely missing. Existing standardization efforts for nanogenerators are AC-type TENGs, such as the universal method proposed by Xia et al. [78]. Based on the effective maximized energy output and Q-V analysis under controlled motion and breakdown conditions, provide a useful starting point but is not directly tailored to DC-type architectures. For DC-TENGs, characterization could be (i) mechanical dynamic inputs (waveform, amplitude, frequency, contact area), (ii) intrinsic DC metrics such as short-circuit current, effective charge collection per cycle, and internal resistance, and (iii) performance under realistic loads, including load-dependent I-V characteristics, matched impedance, and stabilized output power density. Recent studies have also highlighted the importance of reporting time-resolved current traces, derived figures of merit that consider output stability (e.g., peak-to-average behavour), and unified volume/area power densities under well-defined operating conditions, which could be extended as the basis of DC-TENG-specific test recommendations in future TENG community guidelines [23,79–81].

5.6. Hybridization with Other Energy Harvesters

Hybridization is another promising direction for DC-TENGs. Existing demonstrations of DC-TENGs based on hybrid devices, such as wind-driven TENG-EMG systems and multimodal hybrid TENGs, mainly broaden operating bandwidth and improve output through structural and electrical complementation between different harvesters. Combining DC-TENGs to provide high voltage, high-impedance DC outputs that can act as triggers, constant-current contributions, or specific DC bias sources (e.g., corrosion protection or electrochemical processes), while piezoelectric and electromagnetic generators supply AC power, and thermoelectric/photovoltaic devices contribute to low-voltage DC as more continuous baseline sources. These differences in waveform and voltage level necessitate sophisticated multi-input power-management and protection strategies to ensure proper insulation, impedance matching, and coordinated control, and recent advances in high-voltage/constant current and semiconductor-based DC-TENG architectures highlight the opportunity to use DC-TENGs as high-field bias or excitation sources that actively influence charge transport, polarization, or damping in co-integrated harvesters, moving beyond simple power summation towards functionally co-designed hybrid platforms with proper synergies [82,83].

5.7. System-Level Co-Design with Electronics and IoT Protocols

Most current demonstrations integrate DC-TENGs with relatively simple rectifiers, storage capacitors, and regular microcontrollers or wireless modules, without deep co-optimization between harvester, power-management ICs, and communication protocols. For general IoT, it will be important to co-design DC-TENGs with ultra-low-power electronics that support cold-start at high voltage and low current, adaptive maximum power point tracing for pulsed or constant-DC sources, and intermittent or event-driven communication schemes that match harvested energy availability. Integration with edge computing and lightweight machine-learning algorithms could further reduce communication energy by enabling local decision-making and compression sensing [1,2,4,9,10].

5.8. Application-Specific Engineering and Scaling

From an IoT perspective, DC-TENGs must be engineered for specific use cases, body-centric wearables and human-machine interfaces, environmental and agricultural sensing networks, maritime and corrosion-control systems, or distributed electrochemical reactors for hydrogen generation and water treatment [84,85]. Each domain imposes distinct constraints on form factors, mechanical excitation spectrum, environmental robustness, biocompatibility, and regulatory requirements [86,87]. Scaling from single-device demonstrations to dense

networks will demand attention to manufacturing scalability (printing, modeling, role-to-role), low-cost packaging, and modular architectures that allow plug-and-play deployment and maintenance [1,2,6,12,73].

In the longer term, convergence between DC-TENGs and tribotronic/tribovoltaic or iontronic devices may enable chip-level self-powered electronics in which sensing, logic, memory, and power are tightly intertwined. Fabricating such systems will require compatibility with semiconductors and flexible-electronics process flows, as well as robust interfaces between mechanical structures and on-chip devices [10,17,88].

6. Conclusions

DC-TENG has evolved from a simple device concept into a diverse family of mechanisms capable of delivering DC or constant-current output directly from mechanical motion, addressing key limitations of conventional AC-TENGs for IoT applications. By systematically organizing emerging DC-generation routes, air-discharge dielectric breakdown, mechanical delay-switch and rectification, tribovoltaic junction, phase-coupling strategies, iontronic rectification, and ionic-dynamic/electrode polarization effects, and linking them to representative IoT scenarios such as human motion monitoring, smart agriculture, and environmental monitoring, corrosion and cathodic protection, and hydrogen generation, this review clarifies how underlying physics, materials, and architectures translate into system-level capabilities. Looking ahead, advances in interfacial science, durable tribomaterials, mechanism-aware power management circuits, and co-designed ultra-low-power electronics are expected to push DC-TENGs towards practical, large-scale deployment in self-sustained IoT networks. With sustained progress in standardization, hybrid energy-harvesting integration, and application-specific engineering, DC-TENGs have become a key building block in enabling energy-autonomous sensing, computing, and communication across diverse environments.

Author Contributions

S.A.G. and J.-H.L.: concept development; S.A.G.: figures; S.A.G., A.S., and J.-H.L.: writing and editing. All authors have read and agreed to the published version of the manuscript.

Funding

This work was supported by the National Research Foundation of Korea (NRF), funded by the Ministry of Science and ICT (RS-2024-00406674) and the InnoCORE program of the Ministry of Science and ICT (N10250154). Prof. Andris Šutka acknowledges the funding from the Latvian Council of Science in the framework of FLPP “Tribothermoelectric devices with enhanced power output” (lzp-2024/1-0223).

Institutional Review Board Statement

Not applicable.

Informed Consent Statement

Not applicable.

Data Availability Statement

No data was used for the research described in the article.

Conflicts of Interest

Given the role as Editorial Board Member, Ju-Hyuck Lee had no involvement in the peer review of this paper and had no access to information regarding its peer-review process. Full responsibility for the editorial process of this paper was delegated to another editor of the journal.

Use of AI and AI-Assisted Technologies

No AI tools were utilized for this paper.

References

1. Ahmed, A.; Hassan, I.; El-Kady, M.F.; et al. Integrated Triboelectric Nanogenerators in the Era of the Internet of Things. *Adv. Sci.* **2019**, *6*, 1802230. https://doi.org/10.1002/advs.201802230.

2. Cao, X.; Xiong, Y.; Sun, J.; et al. Multidiscipline Applications of Triboelectric Nanogenerators for the Intelligent Era of Internet of Things. *Nano-Micro Lett.* **2023**, *15*, 14. https://doi.org/10.1007/s40820-022-00981-8.
3. Zhao, X.; Askari, H.; Chen, J. Nanogenerators for Smart Cities in the Era of 5G and Internet of Things. *Joule* **2021**, *5*, 1391–1431. https://doi.org/10.1016/j.joule.2021.03.013.
4. Shi, Q.; Sun, Z.; Zhang, Z.; et al. Triboelectric Nanogenerators and Hybridized Systems for Enabling Next-Generation IoT Applications. *Research* **2021**, *2021*, 6849171. https://doi.org/10.34133/2021/6849171.
5. Kim, W.-G.; Kim, D.-W.; Tcho, I.-W.; et al. Triboelectric Nanogenerator: Structure, Mechanism, and Applications. *ACS Nano* **2021**, *15*, 258–287. https://doi.org/10.1021/acsnano.0c09803.
6. Doganay, D.; Durukan, M.B.; Cugunlular, M.; et al. Triboelectric Nanogenerators from Fundamentals to Applications. *Nano Energy* **2025**, *138*, 110825. https://doi.org/10.1016/j.nanoen.2025.110825.
7. Graham, S.A.; Chandrarathna, S.C.; Manchi, P.; et al. Triboelectric Charge Modulation to Understand the Electrification Process in Nanogenerators Combined with an Efficient Power Management System for IoT Applications. *Nano Energy* **2023**, *111*, 108413. https://doi.org/10.1016/j.nanoen.2023.108413.
8. Dong, J.; Zhu, L.; Guo, P.; et al. A Bio-Inspired Total Current Nanogenerator. *Energy Environ. Sci.* **2023**, *16*, 1071–1081. https://doi.org/10.1039/D2EE02621J.
9. Du, S.; Basset, P.; Guo, H.; et al. Power Management Technologies for Triboelectric Nanogenerators. *MRS Bull.* **2025**, *50*, 305–314. https://doi.org/10.1557/s43577-025-00860-8.
10. Ma, W.; Sun, Y.; Wang, C.; et al. Mutual Promotion of Triboelectric Nanogenerators and Field-Effect Transistors towards the IoT. *Nat. Rev. Electr. Eng.* **2025**, *2*, 541–554. https://doi.org/10.1038/s44287-025-00193-3.
11. Wu, Z.; Bi, M.; Cao, Z.; et al. Largely Enhanced Electrostatic Generator Based on a Bipolar Electret Charged by Patterned Contact Micro-Discharge and Optimized Substrates. *Nano Energy* **2020**, *71*, 104602. https://doi.org/10.1016/j.nanoen.2020.104602.
12. Shan, C.; Li, K.; Cheng, Y.; et al. Harvesting Environment Mechanical Energy by Direct Current Triboelectric Nanogenerators. *Nano-Micro Lett.* **2023**, *15*, 127. https://doi.org/10.1007/s40820-023-01115-4.
13. Zhao, Z.; Liu, D.; Li, Y.; et al. Direct-Current Triboelectric Nanogenerator Based on Electrostatic Breakdown Effect. *Nano Energy* **2022**, *102*, 107745. https://doi.org/10.1016/j.nanoen.2022.107745.
14. Gbadam, G.S.; Park, H.; Lee, C.; et al. Direct Current Generation in Triboelectric Nanogenerators through Ionic Dynamics and Electrode Polarization Effects. *Nat. Commun.* **2025**, *16*, 9540. https://doi.org/10.1038/s41467-025-64582-w.
15. Dai, K.; Liu, D.; Yin, Y.; et al. Transient Physical Modeling and Comprehensive Optimal Design of Air-Breakdown Direct-Current Triboelectric Nanogenerators. *Nano Energy* **2022**, *92*, 106742. https://doi.org/10.1016/j.nanoen.2021.106742.
16. Ren, D.; Yang, L.; Zhang, X.; et al. Comprehensive Output Performance Optimization of Ternary Constant DC Triboelectric Nanogenerators via Dual-Phase Symmetric Step-Down Conversion. *Energy Environ. Sci.* **2025**, *18*, 9205–9216. https://doi.org/10.1039/D5EE02837J.
17. Shi, X.; Wang, W.; Wang, J.; et al. Semiconductor-Based Direct Current Triboelectric Nanogenerators and Its Application. *J. Semicond.* **2024**, *45*, 121701. https://doi.org/10.1088/1674-4926/24080021.
18. He, Y.; Tian, J.; Li, F.; et al. Evolution of Tribotronics: From Fundamental Concepts to Potential Uses. *Micromachines* **2024**, *15*, 1259. https://doi.org/10.3390/mi15101259.
19. Zhang, C.; Wang, Z.L. Tribotronics—A New Field by Coupling Triboelectricity and Semiconductor. *Nano Today* **2016**, *11*, 521–536. https://doi.org/10.1016/j.nantod.2016.08.002.
20. Wang, Z.L. From Contact Electrification to Triboelectric Nanogenerators. *Rep. Prog. Phys.* **2021**, *84*, 096502. https://doi.org/10.1088/1361-6633/ac0a50.
21. Liu, D.; Yin, X.; Guo, H.; et al. A Constant Current Triboelectric Nanogenerator Arising from Electrostatic Breakdown. *Sci. Adv.* **2019**, *5*, eaav6437. https://doi.org/10.1126/sciadv.aav6437.
22. Qi, C.; Deng, Y.; Zhi, J.; et al. Output Voltage Enhancement Strategies and Multi-Field Applications of Tribovoltaic Nanogenerators. *ACS Nano* **2025**, *19*, 35212–35236. https://doi.org/10.1021/acsnano.5c09940.
23. Liu, D.; Zhou, L.; Wang, Z.L.; et al. Triboelectric Nanogenerator: From Alternating Current to Direct Current. *iScience* **2021**, *24*, 101932. https://doi.org/10.1016/j.isci.2020.101932.
24. Pathak, M.; Kumar, R. Synchronous Inductor Switched Energy Extraction Circuits for Triboelectric Nanogenerator. *IEEE Access* **2021**, *9*, 76938–76954. https://doi.org/10.1109/ACCESS.2021.3082499.
25. Zhang, J.; Gao, Y.; Liu, D.; et al. Discharge Domains Regulation and Dynamic Processes of Direct-Current Triboelectric Nanogenerator. *Nat. Commun.* **2023**, *14*, 3218. https://doi.org/10.1038/s41467-023-38815-9.
26. Gao, Y.; Liu, D.; Zhou, L.; et al. A Robust Rolling-Mode Direct-Current Triboelectric Nanogenerator Arising from Electrostatic Breakdown Effect. *Nano Energy* **2021**, *85*, 106014. https://doi.org/10.1016/j.nanoen.2021.106014.
27. Liu, J.; Miao, M.; Jiang, K.; et al. Sustained Electron Tunneling at Unbiased Metal-Insulator-Semiconductor Triboelectric Contacts. *Nano Energy* **2018**, *48*, 320–326. https://doi.org/10.1016/j.nanoen.2018.03.052.

28. Liu, J.; Cheikh, M.I.; Bao, R.; et al. Tribo-tunneling DC Generator with Carbon Aerogel/Silicon Multi-nanocontacts. *Adv. Electron. Mater.* **2019**, *5*, 1900464. https://doi.org/10.1002/aelm.201900464.
29. Wang, H.; Huang, S.; Kuang, H.; et al. Coexistence of Contact Electrification and Dynamic p–n Junction Modulation Effects in Triboelectrification. *ACS Appl. Mater. Interfaces* **2022**, *14*, 30410–30419. https://doi.org/10.1021/acsami.2c06374.
30. Meng, J.; Lan, C.; Pan, C.; et al. Coupling of Tribovoltaic Effect and Tribo-Electrostatic Effect at Dynamic Semiconductor Heterojunction Interfaces. *Nano Energy* **2025**, *133*, 110395. https://doi.org/10.1016/j.nanoen.2024.110395.
31. Xu, C.; Yu, J.; Huo, Z.; et al. Pursuing the Tribovoltaic Effect for Direct-Current Triboelectric Nanogenerators. *Energy Environ. Sci.* **2023**, *16*, 983–1006. https://doi.org/10.1039/D2EE04019K.
32. Tian, J.; He, Y.; Li, F.; et al. A Comprehensive Review on the Mechanism of Contact Electrification. *J. Mater. Chem. A* **2025**, *13*, 2505–2536. https://doi.org/10.1039/D4TA07756C.
33. Willatzen, M.; Zhang, Z.; Wang, Z.L. Theory of Tribovoltaics: Direct Current Generation at a p-n Semiconductor Interface. *PRX Energy* **2024**, *3*, 013009. https://doi.org/10.1103/PRXEnergy.3.013009.
34. Ren, L.; Yu, A.; Wang, W.; et al. Pn Junction Based Direct-Current Triboelectric Nanogenerator by Conjunction of Tribovoltaic Effect and Photovoltaic Effect. *Nano Lett.* **2021**, *21*, 10099–10106. https://doi.org/10.1021/acs.nanolett.1c03922.
35. Zhang, Z.; Gong, L.; Luan, R.; et al. Tribovoltaic Effect: Origin, Interface, Characteristic, Mechanism & Application. *Adv. Sci.* **2024**, *11*, 2305460. https://doi.org/10.1002/advs.202305460.
36. Kim, T.; Kim, D.Y.; Yun, J.; et al. Direct-Current Triboelectric Nanogenerator via Water Electrification and Phase Control. *Nano Energy* **2018**, *52*, 95–104. https://doi.org/10.1016/j.nanoen.2018.07.045.
37. Zhang, S.; Li, W.; Li, G.; et al. High Performance DC-TENG Based on Coupling of Mismatched Number of Triboelectric Units and Electrodes with Mechanical Switches for Metal Surface Anti-Corrosion. *Nano Energy* **2024**, *130*, 110093. https://doi.org/10.1016/j.nanoen.2024.110093.
38. Luo, J.; Xu, L.; Tang, W.; et al. Direct-Current Triboelectric Nanogenerator Realized by Air Breakdown Induced Ionized Air Channel. *Adv. Energy Mater.* **2018**, *8*, 1800889. https://doi.org/10.1002/aenm.201800889.
39. Yoon, H.J.; Kang, M.; Seung, W.; et al. Microdischarge-Based Direct Current Triboelectric Nanogenerator via Accumulation of Triboelectric Charge in Atmospheric Condition. *Adv. Energy Mater.* **2020**, *10*, 2000730. https://doi.org/10.1002/aenm.202000730.
40. Zhang, S.; Liu, P.; Zhu, H.; et al. A Highly Efficient Self-Powered Air Purification System Based on High-Voltage-Applicable DC Triboelectric Nanogenerator. *Nano Energy* **2025**, *139*, 110947. https://doi.org/10.1016/j.nanoen.2025.110947.
41. He, W.; Shan, C.; Wu, H.; et al. Capturing Dissipation Charge in Charge Space Accumulation Area for Enhancing Output Performance of Sliding Triboelectric Nanogenerator. *Adv. Energy Mater.* **2022**, *12*, 2201454. https://doi.org/10.1002/aenm.202201454.
42. Jin, B.; Gao, Y.; Liu, D.; et al. Regulation of Discharge Domains and Dynamic Processes in Direct-Current Triboelectric Nanogenerators. *Chem. Eng. J.* **2025**, *512*, 166519. https://doi.org/10.1016/j.cej.2025.166519.
43. Qiao, G.; Wang, J.; Yu, X.; et al. A Bidirectional Direct Current Triboelectric Nanogenerator with the Mechanical Rectifier. *Nano Energy* **2021**, *79*, 105408. https://doi.org/10.1016/j.nanoen.2020.105408.
44. Wu, H.; Wang, S.; Wang, Z.; et al. Achieving Ultrahigh Instantaneous Power Density of 10 MW/m² by Leveraging the Opposite-Charge-Enhanced Transistor-like Triboelectric Nanogenerator (OCT-TENG). *Nat. Commun.* **2021**, *12*, 5470. https://doi.org/10.1038/s41467-021-25753-7.
45. Du, Y.; Fu, S.; Shan, C.; et al. A Novel Design Based on Mechanical Time-Delay Switch and Charge Space Accumulation for High Output Performance Direct-Current Triboelectric Nanogenerator. *Adv. Funct. Mater.* **2022**, *32*, 2208783. https://doi.org/10.1002/adfm.202208783.
46. Zhang, R.; Wang, S.; Yeh, M.-H.; et al. A Streaming Potential/Current-Based Microfluidic Direct Current Generator for Self-Powered Nanosystems. *Adv. Mater.* **2015**, *27*, 6482–6487. https://doi.org/10.1002/adma.201502477.
47. Chi, J.; Liu, C.; Che, L.; et al. Harvesting Water-Evaporation-Induced Electricity Based on Liquid–Solid Triboelectric Nanogenerator. *Adv. Sci.* **2022**, *9*, 2201586. https://doi.org/10.1002/advs.202201586.
48. Zhang, Z.; Jiang, D.; Zhao, J.; et al. Tribovoltaic Effect on Metal–Semiconductor Interface for Direct-Current Low-Impedance Triboelectric Nanogenerators. *Adv. Energy Mater.* **2020**, *10*, 1903713. https://doi.org/10.1002/aenm.201903713.
49. Shi, K.; Chai, B.; Zou, H.; et al. Direct-Current Triboelectric Nanogenerators Based on Contact–Separation Mode and Conductive–Adhesive Interface. *Adv. Funct. Mater.* **2024**, *34*, 2400204. https://doi.org/10.1002/adfm.202400204.
50. Ouyang, Y.; Wang, Z.L.; Wei, D. Ionic Rectification via Electrical Double Layer Modulation at Hydrogel Interfaces. *RSC Appl. Interfaces* **2025**, *2*, 873–896. https://doi.org/10.1039/D5LF00098J.
51. Li, X.; Wang, Z.L.; Wei, D. Nanogenerators via Dynamic Regulation of Electrical Double Layer. *Nano Trends* **2024**, *7*, 100062. https://doi.org/10.1016/j.nwnano.2024.100062.
52. Wei, Y.; Li, X.; Gu, Y.; et al. Probing Electrical Double Layer via Triboelectric Charge Transfer. *Nat. Commun.* **2026**, *17*, 402. https://doi.org/10.1038/s41467-025-67094-9.

53. Ouyang, Y.; Li, X.; Li, S.; et al. Opto-Iontronic Coupling in Triboelectric Nanogenerator. *Nano Energy* **2023**, *116*, 108796. https://doi.org/10.1016/j.nanoen.2023.108796.
54. Liu, G.; Fan, B.; Qi, Y.; et al. Ultrahigh-Current-Density Tribovoltaic Nanogenerators Based on Hydrogen Bond-Activated Flexible Organic Semiconductor Textiles. *ACS Nano* **2025**, *19*, 6771–6783. https://doi.org/10.1021/acsnano.4c11010.
55. Luo, Q.; Xiao, K.; Zhang, J.; et al. Direct-Current Triboelectric Nanogenerators Based on Semiconductor Structure. *ACS Appl. Electron. Mater.* **2022**, *4*, 4212–4230. https://doi.org/10.1021/acsaelm.2c00758.
56. Rahman, M.T.; Kim, Y.-S.; Rahman, M.S.; et al. Bimetallic Nanoporous Carbon-Based Direct-Current Triboelectric Nanogenerators for Biomechanical Energy Harvesting and Sensing. *Chem. Eng. J.* **2025**, *519*, 164938. https://doi.org/10.1016/j.cej.2025.164938.
57. Wang, J.; Wang, X.; Lee, J.P.; et al. Nanogenerators Developed Based on Different Physics Effects. *MRS Bull.* **2025**, *50*, 271–281. https://doi.org/10.1557/s43577-024-00857-9.
58. Kim, M.P.; Lee, Y.; Hur, Y.H.; et al. Molecular Structure Engineering of Dielectric Fluorinated Polymers for Enhanced Performances of Triboelectric Nanogenerators. *Nano Energy* **2018**, *53*, 37–45. https://doi.org/10.1016/j.nanoen.2018.08.048.
59. Kim, M.P.; Um, D.-S.; Shin, Y.-E.; et al. High-Performance Triboelectric Devices via Dielectric Polarization: A Review. *Nanoscale Res. Lett.* **2021**, *16*, 35. https://doi.org/10.1186/s11671-021-03492-4.
60. Dong, J.; Xu, C.; Zhu, L.; et al. A High Voltage Direct Current Droplet-Based Electricity Generator Inspired by Thunderbolts. *Nano Energy* **2021**, *90*, 106567. https://doi.org/10.1016/j.nanoen.2021.106567.
61. Liu, T.; Mo, W.; Zou, X.; et al. Liquid–Solid Triboelectric Probes for Real-Time Monitoring of Sucrose Fluid Status. *Adv. Funct. Mater.* **2023**, *33*, 2304321. https://doi.org/10.1002/adfm.202304321.
62. Guan, Q.; Zhu, Z.; Song, Y.; et al. A Multifunctional Self-Charging System Based on a Compatible Electrode. *ACS Appl. Mater. Interfaces* **2025**, *17*, 55318–55327. https://doi.org/10.1021/acsami.5c11100.
63. Fu, S.; He, W.; Wu, H.; et al. High Output Performance and Ultra-Durable DC Output for Triboelectric Nanogenerator Inspired by Primary Cell. *Nano-Micro Lett.* **2022**, *14*, 155. https://doi.org/10.1007/s40820-022-00973-8.
64. Lei, K.; Liu, C.; Wang, Y.; et al. Research on a Dual-Effect DC Ocean Energy Harvesting System Combining the Ternary Dielectric Effect and the Seebeck Effect. *Adv. Sustainable Syst.* **2025**, *9*, e00591. https://doi.org/10.1002/adsu.202500591.
65. Kang, Y.; Wu, H.; Yi, H.; et al. Surface Non-Equilibrium State Induced by Unipolar Charge Collection for Constructing Constant Current Power Generation. *Adv. Funct. Mater.* **2025**, *35*, 2505503. https://doi.org/10.1002/adfm.202505503.
66. Lee, M.-H. Wearable Strain Sensor and Flexible Direct-Current Nanogenerator Made by Medical Mask Wastes and PEDOT: PSS-Based Conductive Inks. *Sustain. Mater. Technol.* **2025**, *44*, e01400. https://doi.org/10.1016/j.susmat.2025.e01400.
67. Kim, J.; Yoo, J.; Seo, H.; et al. Magnetically Driven Triboelectric Nanogenerator for a Wireless, Versatile Energy Transfer System. *Sci. Adv.* **2025**, *11*, eadu5919. https://doi.org/10.1126/sciadv.adu5919.
68. Zhao, Z.; Wang, J. Advances in Interfacial Electrostatic Energy Harvesting via Direct Current Triboelectric Nanogenerators. *Adv. Energy Mater.* **2025**, *15*, 2502544. https://doi.org/10.1002/aenm.202502544.
69. Guo, X.; You, J.; Wei, D.; et al. A Generalized Model for Tribovoltaic Nanogenerator. *Appl. Phys. Rev.* **2024**, *11*, 021406. https://doi.org/10.1063/5.0196998.
70. Callaty, C.; Rodrigues, C.; Ventura, J. Triboelectric Nanogenerators in Harsh Conditions: A Critical Review. *Nano Energy* **2025**, *140*, 110661. https://doi.org/10.1016/j.nanoen.2025.110661.
71. Zhao, J.; Shi, Y. Boosting the Durability of Triboelectric Nanogenerators: A Critical Review and Prospect. *Adv. Funct. Mater.* **2023**, *33*, 2213407. https://doi.org/10.1002/adfm.202213407.
72. Somkuwar, V.U.; Garg, H.; Maurya, S.K.; et al. Influence of Relative Humidity and Temperature on the Performance of Knitted Textile Triboelectric Nanogenerator. *ACS Appl. Electron. Mater.* **2024**, *6*, 931–939. https://doi.org/10.1021/acsaelm.3c01442.
73. Manojkumar, K.; Muthuramalingam, M.; Hajra, S.; et al. Direct Current Triboelectric Nanogenerator Nexus: Fundamentals to Applications in Self-Powered Systems. *Nano Energy* **2025**, *147*, 111148. https://doi.org/10.1016/j.nanoen.2025.111148.
74. Yin, X.; Chen, Z.; Chen, H.; et al. Optimization Strategy of Triboelectric Nanogenerators for High Humidity Environment Service Performance. *EcoMat* **2024**, *6*, e12493. https://doi.org/10.1002/eom2.12493.
75. Graham, S.A.; Chandrarathna, S.C.; Patnam, H.; et al. Harsh Environment–Tolerant and Robust Triboelectric Nanogenerators for Mechanical-Energy Harvesting, Sensing, and Energy Storage in a Smart Home. *Nano Energy* **2021**, *80*, 105547. https://doi.org/10.1016/j.nanoen.2020.105547.
76. Peng, J.; Kang, S.D.; Snyder, G.J. Optimization Principles and the Figure of Merit for Triboelectric Generators. *Sci. Adv.* **2017**, *3*, eaap8576. https://doi.org/10.1126/sciadv.aap8576.
77. Lee, Y.-S.; Jeon, S.; Kim, D.; et al. High Performance Direct Current-Generating Triboelectric Nanogenerators Based on Tribovoltaic p-n Junction with ChCl-Passivated CsFAMA Perovskite. *Nano Energy* **2023**, *106*, 108066. https://doi.org/10.1016/j.nanoen.2022.108066.
78. Xia, X.; Fu, J.; Zi, Y. A Universal Standardized Method for Output Capability Assessment of Nanogenerators. *Nat. Commun.* **2019**, *10*, 4428. https://doi.org/10.1038/s41467-019-12465-2.

79. Li, Z.; Yang, C.; Zhang, Q.; et al. Standardized Volume Power Density Boost in Frequency-Up Converted Contact-Separation Mode Triboelectric Nanogenerators. *Research* **2023**, *6*, 0237. https://doi.org/10.34133/research.0237.
80. Li, Q.; Fu, S.; Yang, H.; et al. Achieving Ultrahigh DC-Power Triboelectric Nanogenerators by Lightning Rod-Inspired Field Emission Modeling. *Research* **2024**, *7*, 0437. https://doi.org/10.34133/research.0437.
81. You, Z.; Wang, S.; Li, Z.; et al. High Current Output Direct-Current Triboelectric Nanogenerator Based on Organic Semiconductor Heterojunction. *Nano Energy* **2022**, *91*, 106667. https://doi.org/10.1016/j.nanoen.2021.106667.
82. Luo, Q.; Xiao, K.; Li, M.; et al. Metal-Semiconductor Direct-Current Triboelectric Nanogenerator Based on Depletion Mode u-GaN/AlGaN/AlN/GaN HEMT. *Appl. Phys. Lett.* **2023**, *123*, 063901. https://doi.org/10.1063/5.0158240.
83. Zhang, W.; Gui, Y.; Yang, Y.; et al. A Hybrid Nanogenerator Based on Wind Energy Harvesting for Powering Self-Driven Sensing Systems. *J. Cleaner Prod.* **2023**, *429*, 139550. https://doi.org/10.1016/j.jclepro.2023.139550.
84. Nan, Y.; Wang, X.; Xu, H.; et al. Customizing Alternating and Direct Current Dual-Mode Solid-Liquid Triboelectric Nanogenerator. *Nano Energy* **2025**, *137*, 110812. https://doi.org/10.1016/j.nanoen.2025.110812.
85. Zhu, Z.; Wang, M.; Wang, A.; et al. Improved Self-Sensing Harsh-Impact Absorber Merging Compression-Torsion Metamaterial with Active Magnetorheological Effects. *Nano Energy* **2025**, *139*, 110921. https://doi.org/10.1016/j.nanoen.2025.110921.
86. Xia, J.; Li, H.; Song, Y.; et al. "Triboelectric Immunotherapy" Powered Osteogenesis and Osteoimmune Reprogramming for Graft-Free Repair of Bone Defects. *Chem. Eng. J.* **2025**, *506*, 171006. https://doi.org/10.1016/j.cej.2025.171006.
87. Wang, S.; Lu, F.; Guan, W.; et al. Energy Harvesting from Clothing. *Nanoscale* **2025**, *17*, 7986–7996. https://doi.org/10.1039/D4NR03719G.
88. Zhang, C.; Zhao, J.; Zhang, Z.; et al. Tribotronics: An Emerging Field by Coupling Triboelectricity and Semiconductors. *Int. J. Extreme Manuf.* **2023**, *5*, 042002. https://doi.org/10.1088/2631-7990/ace669.